Statistical Mechanics of Liquid He⁴†*

RYOICHI KIKUCHI,‡ HARRY H. DENMAN, AND CHARLES L. SCHREIBER§
Department of Physics, Wayne State University, Detroit, Michigan
(Received May 4, 1960)

The partition function proposed by Feynman for liquid He⁴, based on his path integral method, is evaluated for a simple cubic lattice considering long-range permutations as well as nearest-neighbor permutations (to which the previous analysis by one of the authors was restricted). The result indicates a second-order phase transition at the λ point. The marked improvements over the previous treatment are: (1) the specific heat behaves as T^3 near absolute zero, (2) the specific heat peak is more pronounced at the λ point, and (3) when triangles are added as possible finite polygons above T_λ the specific heat just above T_λ increases over the previous result, showing an improvement. Equating the theoretical λ point with the experimental, a value for the effective mass of a helium atom about 1.6 times the normal mass is obtained.

1. INTRODUCTION

APPLYING his path-integral approach[1] to quantum statistical mechanics, Feynman[2,3] has shown that the partition function of a system of He⁴ atoms can be written in a form equivalent to that for a group of atoms of effective mass m' in fictitious motion between various permutations of the helium atoms. Using certain experimentally known characteristics of liquid He⁴, he derived a third-order phase transition between two liquid phases, and succeeded in obtaining some other qualitative features of the specific heat curve. Experimentally, however, the transition at the λ point is not of third order, and also many properties of the observed specific heat remained to be explained.

Adopting Feynman's expression for the partition function and assuming a simple cubic lattice structure for the liquid, one of the authors,[4] applying techniques developed earlier for cooperative phenomena, considered in detail correlation effects between nearest-neighboring atoms, and found a second-order phase change at the λ point.

The specific heat, as obtained in (I), was based on the part q of the partition function Q given by Eq. (7) of reference 3:

$$Q=q(K_\beta/N!)(m'kT/2\pi\hbar^2)^{3N/2}. \quad (1.1)$$

In (I), the factors following q were omitted in calculating the specific heat because the main interest was whether the transition would be of the second or the third order, and these factors were believed to be continuous functions of temperature and to have no effect on the order of the transition. If one ignores the temperature dependence of K_β (see Sec. 6), but includes the effect of $T^{3N/2}$, the specific heat curve of (I) becomes as shown with the dashed curve in Fig. 6.

Qualitatively, this curve does not behave properly as T approaches 0°K and also just above T_λ, since experimentally the specific heat approaches zero as T^3 near 0°K, and decreases monotonically as T increases above the transition point. The present paper treats correlations between the atoms of the lattice model more accurately, and derives an expression for the specific heat which has the correct qualitative behavior as T approaches 0°K and which has improved behavior above T_λ, while preserving the second-order phase transition.

2. NECESSITY FOR LONG-SIDED POLYGONS

When one applies Feynman's path integral approach to quantum statistical mechanics, the essential mathematical problem is to sum Boltzmann factors over all possible configurations of polygons in space.[3,4] A polygon, as will be explained in detail below, is defined as a closed chain of permutations among atoms of the lattice. In (I), it was assumed that a side of a polygon linked only nearest-neighbor lattice points, as shown in Fig. 1. We call this side, whose length is that of the lattice constant, a *short side*. This assumption on the length of a side was based on mathematical convenience. Polygons with longer sides are as important as those with short sides, but were omitted in (I) only because the inclusion of them was imagined to make calculation

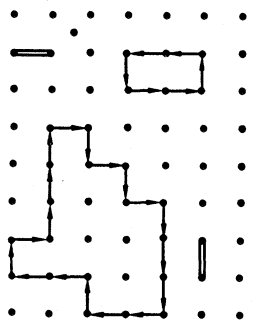

FIG. 1. Examples of short-sided polygons in the lattice model of liquid He⁴ treated in (I).

† This work was supported in part by the U. S. Department of Defense.
* A preliminary report of this work was presented at the Summer Meeting of the American Physical Society on June 20, 1959 at Milwaukee, Wisconsin. See Bull. Am. Phys. Soc. 4, 327 (1959).
‡ Now at Hughes Aircraft Company, Malibu, California.
§ Now at Department of Physics, University of California, Los Angeles, California.
[1] R. P. Feynman, Revs. Modern Phys. **20**, 367 (1948).
[2] R. P. Feynman, Phys. Rev. **90**, 1116 (1953).
[3] R. P. Feynman, Phys. Rev. **91**, 1291 (1953).
[4] R. Kikuchi, Phys. Rev. **96**, 563 (1954), hereafter referred to as (I), and regarded as Part I of this paper.

CONFIGURATION	PROBABILITY	WEIGHT β_i
• •	y_1	1
• ⊂	y_2	10
⇒ ∪	y_3	25
⊂⊃	y_4	1
• ⌊	y_5	40
⇒ ⌊	y_6	200
⌊ ⌐	y_7	400
⌊⌋	y_8	50

FIG. 2. First set of pair probability parameters (simple cubic lattice treatment) used in (I).

intractable, and also because the emphasis in (I) was on the existence of a second order transition point.

This limitation on the length of a side is tolerable near and above T_λ for the following reason. A side (of a polygon) of length l contributes a virtual energy of[3]

$$\epsilon_l^* = m'(lkT)^2/2\hbar^2, \tag{2.1}$$

or a Boltzmann factor $\exp(-m'l^2kT/2\hbar^2)$. Here the effective mass m' is of the order of twice the actual mass of a He^4 atom. It can be seen that ϵ_l^*/kT is about unity when T is the observed T_λ and l is the average nearest-neighbor distance between atoms in liquid He^4. This means the Boltzmann factor becomes much smaller than unity as the length of a side increases beyond the nearest-neighbor distance of the atoms, which is approximately the lattice constant in the lattice model of Feynman.

However, for a temperature much lower than the observed λ point, ϵ_l^* of (2.1) decreases and the Boltzmann factor $\exp(-\epsilon_l^*/kT)$ approaches unity even for large values of l. For this reason the approximation of (I) becomes poor as T approaches absolute zero. Then it is clear that the result may be expected to improve as one includes long-sided polygons in the calculation. (In this paper a side longer than the nearest-neighbor lattice distance will be called a *long side.*)

CONFIGURATION	PROBABILITY	WEIGHT β_i
• △	y_9	20
• ○	y_{10}	2
⇒ △	y_{11}	100
⇒ ○	y_{12}	10
⌊ △	y_{13}	400
⌊ ○	y_{14}	40
◁ ⌊	y_{15}	100
◁ ○	y_{16}	20
⌊ △	y_{17}	20
△ △	y_{18}	2
○ ○	y_{19}	1

FIG. 3. Second set of pair probability parameters. → is a short side. – – – – or – – – – → is a long side. △ connects a long side with a short side. ○ is a lattice point between two long sides.

3. DEFINITION OF PARAMETERS

For the pair approximation treatment used in (I) the probability parameters shown in Fig. 2 were used.

CONFIGURATION	PROBABILITY	WEIGHT a_i
•	x_1	1
⇒	x_2	6
⌊	x_3	30
⌊ △	x_4	12
○	x_5	1

FIG. 4. Point probability parameters (simple cubic lattice).

In order to take into account polygons with longer sides, the additional parameters defined in Fig. 3 are introduced, where a broken line indicates a long side. In these figures, an arrow indicates the direction of permutation. At a triangle lattice point △ a long side meets a short side. An open circle ○ is a lattice point where two long sides meet. In counting β_i in Fig. 3, the two different directions for a long side (when there is no arrow attached to it) are not counted. For long sides, – – – – or – – – – →, neither lengths nor spatial directions are specified. The configurations for one lattice point are shown in Fig. 4. Only x_1 x_2, and x_3 were used in (I).

Let N_l be the total number of long sides of length l in the system. It satisfies the following relation

$$\sum_{l>c}^{l_{\max}} N_l = N(6x_4+x_5) = \hat{N}, \tag{3.1}$$

where c is the lattice constant of the simple cubic lattice and N the total number of lattice points (atoms) in the system. Since the need arises later, the quantity $\hat{N}$, which is the total number of long sides, is defined in (3.1). The factor $6x_4+x_5$ comes from the consideration

that a configuration in which a long side comes *into* a triangle point and a short side goes *out* has the probability x_4 and weight 6, and a circle lattice point has the probability x_5 and weight unity.

Using these parameters, the virtual energy E^* of the system becomes

$$E^*=3N\epsilon_c^*(2y_4+50y_8+20y_{17}+2y_{18})+\sum_{l>c}^{l_{\max}}\epsilon_l^* N_l. \quad (3.2)$$

Here the first term comes from the short sides and the second from the long sides.

Brush[5] has emphasized that the virtual energy for a double-sided polygon is different from twice the value for a single side. This difference is not taken into account in the present paper, however, in order not to complicate unduly the mathematics, since the main object of the present work is to discover the effect of adding the long-sided polygons.

4. COMBINATORIAL FACTOR

Using Figs. 2 through 4, one may extend the combinational g factor of Eq. (5) of (I) and write for a system of N lattice points:

$$g=[\prod_{i=1}^{5}(x_iN)!^{\alpha_i}]^5[\prod_{i=1}^{19}(y_iN)!^{\beta_i}]^{-3}N!^{-2}. \quad (4.1)$$

But in the present case this is not the correct weight factor, because configurations of long sides have not been included. This point will be clarified by the following illustration. Equation (4.1) counts only the skeletons like Fig. 5(a). When one draws the long sides on it, there are many possible configurations; two of these are shown in Figs. 5(b) and (c). In other words, when the factor q of (1.1) is written in the form

$$q=G(\{x_i\},\{y_i\},\{N_l\})\times\exp[-E^*(\{x_i\},\{y_i\},\{N_l\})/kT], \quad (4.2)$$

the weight factor G is now given by

$$G=g\Gamma, \quad (4.3)$$

where Γ comes from distributions of long sides over a pattern like Fig. 5(a).

The factor Γ is calculated in terms of N_l in the following way. Let $\bar{N}_l$ be the total number of lattice points of the type △ or ○ which can be reached by an arrow of length l starting from a lattice point △ or ○ in Fig. 4. (As is seen in Fig. 4, either △ or ○ can be a starting point for a long side.) In actuality, $\bar{N}_l$ varies from point to point, but it is assumed that $\bar{N}_l$ is the same for every point △ or ○. Then, on the average,

$$\bar{N}_l=(6x_4+x_5)N_l^{(0)}, \quad (4.4)$$

where $N_l^{(0)}$ is the number of *lattice* points which lie at a distance l from a certain lattice point. $N_l^{(0)}$ is a purely geometrical quantity and a few examples for a simple cubic lattice are $N_l^{(0)}=12$ for $l=\sqrt{2}c$, and $N_l^{(0)}=8$ for $l=\sqrt{3}c$.

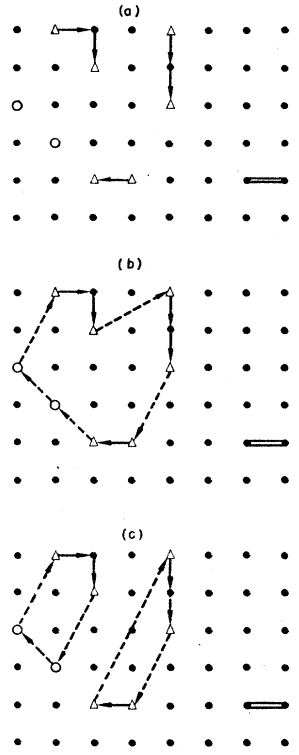

FIG. 5. Methods of constructing polygons of long and short sides. (a) Short sides only. (b) Long sides added. (c) Alternative pattern for the added long sides.

Suppose a distribution such as is shown in Fig. 5(a) has been completed and now the long-sided polygons are to be filled in. The total number of long sides to be drawn is $\hat{N}$. We may draw the long sides in the following way. First we draw N_{l_1} long sides of the length l_1, then N_{l_2} sides of the length l_2, etc. The number of ways, Γ_{l_1}, of drawing N_{l_1} long sides of the length l_1 is counted as follows. The number of ways of drawing the first long side is $\hat{N}\bar{N}_{l_1}$, because there are $\hat{N}$ lattice points from which the side can begin and for each of these points there are $\bar{N}_{l_1}$ points where it may end. For the next long side, the number of available lattice points where it may begin is now $\hat{N}-1$ and for each of these points there are $\bar{N}_{l_1}(1-1/\hat{N})$ possible end points on the average, so that the number of ways of drawing the second long side of length l_1 is $(\hat{N}-1)\times\bar{N}_{l_1}(1-1/\hat{N})$. Similarly, for the $(\nu+1)$th long side of length l_1, the number of ways of drawing it is

$$(\hat{N}-\nu)\bar{N}_{l_1}(1-\nu/\hat{N}). \quad (4.5)$$

Thus Γ_{l_1} becomes

$$\Gamma_{l_1}=(N_{l_1}!)^{-1}\prod_{\nu=0}^{N_{l_1}-1}(\hat{N}-\nu)^2\bar{N}_{l_1}/\hat{N}. \quad (4.6)$$

The division by $N_{l_1}!$ arises because the final configuration is independent of the choice of the order of N_{l_1} sides.

[5] S. G. Brush, Proc. Roy. Soc. (London) **A242**, 544 (1957); **A247**, 225 (1958).

For the number of ways Γ_{l_2} of the drawing N_{l_2} sides of the length l_2, the available number of lattice points to start with is $\hat{N}-N_{l_1}$ so that

$$\Gamma_{l_2}=(N_{l_2}!)^{-1}\prod_{\nu=N_{l_1}}^{N_{l_1}+N_{l_2}-1}(\hat{N}-\nu)^2\bar{N}_{l_2}/\hat{N}. \quad (4.7)$$

The total number of ways of drawing all the long sides can be obtained by multiplying together the factors Γ_{l_i}:

$$\Gamma=\prod_i\Gamma_{l_i}=[\prod_{l>c}^{l_{\max}}N_l!]^{-1}(\hat{N}!)^2 \times\exp(-\hat{N}\ln\hat{N})\prod_{l>c}^{l_{\max}}(\bar{N}_l)^{N_l}. \quad (4.8)$$

This expression multiplied by g of (4.1) gives the desired G factor as shown in (4.3). Using Stirling's formula and taking the logarithm, it follows from (4.8) that

$$\ln\Gamma=\hat{N}\ln\hat{N}-\hat{N}+\sum_{l>c}^{l_{\max}}N_l(\ln\bar{N}_l-\ln N_l). \quad (4.9)$$

5. FREE ENERGY

For the lattice model treated here, the free energy is expressed as follows:

$$F=-kT\ln[K_\beta N!^{-1}(m'kT/2\pi\hbar^2)^{3N/2}] +E^*-kT\ln G, \quad (5.1)$$

where the first term is due to the coefficient of q in Eq. (1.1), E^* is given in Eq. (3.2) and G in (4.3). K_β is a function of temperature for which Feynman[3] derived the relation

$$K_\beta=V^N/V_N, \quad (5.2)$$

where V is the volume of the system and V_N is the "free volume" for the N atoms in the system. As long as the system remains liquid, it is expected that K_β will not change much.

The F in (5.1) may be written as

$$\begin{aligned}F/kT&=-\ln[K_\beta N!^{-1}(m'kT/2\pi\hbar^2)^{3N/2}]\\&\quad+3N\tau(2y_4+50y_8+20y_{17}+2y_{18})\\&\quad-5N\sum_{i=1}^{5}\alpha_ix_i\ln x_i+3N\sum_{i=1}^{18}\beta_iy_i\ln y_i+F'/kT, \quad (5.3)\end{aligned}$$

where

$$F'/kT=\sum_{l>c}^{l_{\max}}\tau N_l l^2/c^2-\hat{N}\ln\hat{N}+\hat{N} -\sum_{l>c}^{l_{\max}}N_l(\ln\bar{N}_l-\ln N_l)-\lambda[\bar{N}-\sum_{l>c}^{l_{\max}}N_l], \quad (5.4)$$

and

$$\tau=m'c^2kT/2\hbar^2 \quad (5.5)$$

is a dimensionless quantity proportional to the temperature. λ in the last term of (5.4) is the Lagrange multiplier for the condition (3.1). This F in (5.3) is a function of the probability parameters $\{x_i\}$, $\{y_i\}$, and $\{N_l\}$, and will be minimized with respect to these parameters.

F is separated in (5.3) so that N_l appears only in F'. First F or F' is minimized with respect to N_l, with the result

$$N_l=\bar{N}_l\exp[-\tau l^2/c^2-(\lambda+1)]. \quad (5.6)$$

The multiplier λ is determined from Eq. (3.1) and (4.4) as

$$e^{\lambda+1}=N^{-1}\sum_{l>c}^{l_{\max}}N_l^{(0)}\exp(-\tau l^2/c^2). \quad (5.7)$$

$N_l^{(0)}$ was defined below Eq. (4.4). Its meaning allows one to transform (5.7) into

$$e^{\lambda+1}=N^{-1}\{\sum_{n_1,n_2,n_3=-\infty}^{\infty}\exp[-(n_1^2+n_2^2+n_3^2)\tau] -1-6e^{-\tau}\}, \quad (5.8)$$

where n_1, n_2, and n_3 are integers. (Notice that a simple cubic lattice is assumed for this expression.) Using the definition of the θ_3 function[6]:

$$\vartheta_3(x;e^{-\tau})=\sum_{n=-\infty}^{\infty}\exp(-n^2\tau+2\pi inx), \quad (5.9)$$

one can write (5.8) as

$$B=Ne^{\lambda+1}=[\vartheta_3(0;e^{-\tau})]^3-1-6e^{-\tau}. \quad (5.10)$$

When (5.6) is satisfied, one can write (5.4) as

$$F'/kT=-\hat{N}\ln\hat{N}-\lambda\hat{N}. \quad (5.11)$$

Equations (3.1) and (5.10) transform this into

$$F'/kT=N(6x_4+x_5)[-\ln(6x_4+x_5)+1-\ln B]. \quad (5.12)$$

Then (5.3) becomes

$$\begin{aligned}F/NkT&=-\ln[(K_\beta/N!)^{1/N}(m'kT/2\pi\hbar^2)^{\frac{3}{2}}]\\&\quad+3\tau(2y_4+50y_8+20y_{17}+2y_{18})\\&\quad-5\sum_{i=1}^{5}\alpha_ix_i\ln x_i+3\sum_{i=1}^{19}\beta_iy_i\ln y_i\\&\quad+(6x_4+x_5)[-\ln(6x_4+x_5)+1-\ln B]. \quad (5.13)\end{aligned}$$

This is a function of x_i and y_i only, since N_l has been eliminated. The next step is to minimize F in (5.13) with respect to the independent x_i and y_i. Before doing this, it is worthwhile to write another form of the function B. Using an alternative expression for the ϑ_3 function[6]:

$$\vartheta_3(x;e^{-\tau})=(\pi/\tau)^{\frac{1}{2}}\sum_{n=-\infty}^{\infty}\exp[-\pi^2(x+n)^2/\tau], \quad (5.14)$$

[6] See, for instance, E. T. Whittaker and G. N. Watson, *Modern Analysis* (Cambridge University Press, Cambridge and the McMillan Company, New York, 1946), Chap. 21.

one transforms (5.10) into

$$B=(\pi/\tau)^{\frac{3}{2}}\{[\sum_{n=-\infty}^{\infty}\exp(-\pi^2n^2/\tau)]^3 - (\tau/\pi)^{\frac{3}{2}}(1+6e^{-\tau})\}. \quad (5.15)$$

This expression is particularly important when one discusses the behavior of the system near 0°K.

6. MINIMIZATION OF FREE ENERGY

The next procedure is the minimization of F, Eq. (5.13), with respect to the independent probability parameters. Among the parameters x_i and y_i defined in Figs. 2, 3, and 4, there are the following relations:

$$\begin{aligned}
&1=x_1+6x_2+30x_3+12x_4+x_5,\\
&x_1=y_1+5y_2+20y_5+10y_9+y_{10},\\
&x_2=y_2+5y_3+20y_6+10y_{11}+y_{12}=y_4,\\
&x_3=y_5+5y_6+20y_7+10y_{13}+y_{14}=5y_8+y_{17},\\
&y_4=y_9+5y_{11}+20y_{13}+10y_{15}+y_{16}=5y_{17}+y_{18},\\
&x_5=y_{10}+5y_{12}+20y_{14}+10y_{16}+y_{19}.
\end{aligned} \quad (6.1)$$

Out of the 24 quantities x_i and y_i, 15 are independent. Choosing a set of 15 parameters as independent, one can minimize the free energy, obtaining 15 higher order algebraic equations which are then solved simultaneously. The details of this mathematical procedure will be omitted here, but the final equation is the following for a variable α:

$$\alpha^5-\alpha^4(Be^{\tau}+3)-\alpha^3(Be^{\tau}+14+2e^{\tau}) +5\alpha^2(Be^{\tau}+2+2e^{\tau})+5\alpha(Be^{\tau}+9)+25=0. \quad (6.2)$$

Here α is defined by

$$\alpha\equiv 5+(z_{10}/z_5)^{\frac{1}{2}}, \quad (6.3)$$

where

$$z_i=y_i/y_1 \quad \text{for} \quad i=2,3,\cdots,19. \quad (6.4)$$

After α is obtained from (6.2) the probability parameters x_i and y_i are found from the following relations:

$$\begin{aligned}
&x_1=(\alpha-5)/[B(\alpha+1)],\\
&x_2=z_2x_1,\\
&x_3=z_5x_1,\\
&x_4=z_9z_1,\\
&x_5=z_{10}x_1,\\
&y_1=(\alpha-5)e^{\tau}/[B\alpha(\alpha+1)],\\
&z_2=e^{-\tau}/\alpha,\\
&z_3=z_2^2,\\
&z_4=e^{-2\tau},\\
&z_5=(\alpha^2e^{-\tau}-\alpha-5e^{-\tau})/[\alpha(\alpha^2-5)],\\
&z_6=z_2z_5,\\
&z_7=z_5^2,\\
&z_8=z_5e^{-\tau},\\
&z_9=(z_5z_{10})^{\frac{1}{2}},\\
&z_{10}=z_5(\alpha-5)^2,\\
&z_{11}=z_2z_9,\\
&z_{12}=z_2z_{10},\\
&z_{13}=z_5z_9,\\
&z_{14}=z_5z_{10},\\
&z_{15}=z_9^2,\\
&z_{16}=z_9z_{10},\\
&z_{17}=(z_5z_{10})^{\frac{1}{2}}e^{-\tau},\\
&z_{18}=z_{10}e^{-\tau},\\
&z_{19}=z_{10}^2.
\end{aligned} \quad (6.5)$$

When these results are substituted in (5.13), F becomes

$$F=NkT\{-\ln[(K_\beta/N!)^{1/N}(m'kT/2\pi\hbar^2)^{\frac{3}{2}}] -5\ln x_1+3\ln y_1+6x_4+x_5\}. \quad (6.6)$$

The entropy S is derived from (5.13) by differentiation[7]:

$$S=-\frac{\partial F}{\partial T}=-\frac{F}{T}+kT\partial\ln K_\beta/\partial T+\tfrac{3}{2}Nk -3Nk\tau(2y_4+50y_2+20y_{17}+2y_{18}) +NkT(6x_4+x_5)\partial\ln B/\partial T. \quad (6.7)$$

The energy E is

$$E=F+TS =kT^2\partial\ln K_\beta/\partial T+\tfrac{3}{2}NkT -6NkT\tau(y_4+25y_8+10y_{17}+y_{18}) +NkT^2(6x_4+x_5)\partial\ln B/\partial T. \quad (6.8)$$

It should be noted that this is the true energy of a system, whereas E^* of (3.2) is a virtual energy.

In the expression for the energy, the first term depends on the temperature gradient of K_β. This quantity K_β has not been fully analyzed, but Feynman has written it in terms of V_N [see (5.2)], which in turn is defined in Eq. (10) of reference 3 as

$$V_N=\int\rho(z^N)d^Nz_i. \quad (6.9)$$

Here z^N represents the coordinates of the N atoms and $\rho(z^N)$ is the weight function corresponding to a spatial configuration z^N. In so far as the system stays liquid, the weight function $\rho(z^N)$ will not depend strongly on the temperature, resulting in small temperature dependence for K_β. Because of this presumption and also because of the lack of detailed knowledge of K_β, the first term of (6.8) will be neglected hereafter.

[7] The expression (6.6) is not convenient to use here, because if one uses it, one has to differentiate x_1, y_1, x_4, and x_5 with respect to T also. Equation (5.13) is convenient because it is known that derivatives of (5.13) with respect to the independent variables vanish.

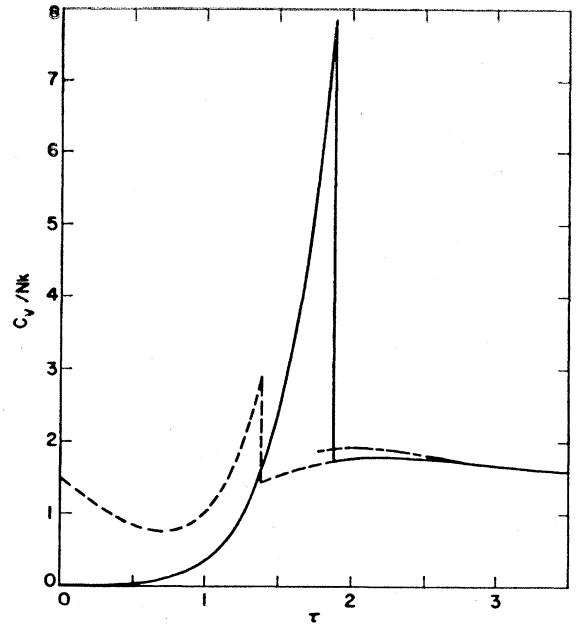

FIG. 6. Specific heat vs temperature. The solid curve: Sec. 9 of this paper. The dashed curve: previous paper (I). The dot-dash curve: Sec. 10 of this paper.

7. THE λ POINT

As τ is varied (and thus T), one obtains, from Eq. (5.10) and (6.2) to (6.5), values of the probability parameters $\{x_i\}$ and $\{y_i\}$ for each assumed value of τ. As the value of τ is increased from zero, one finds a point where the probability parameters x_3 to x_5 and y_5 to y_{19} become zero. Any further increase in τ, using these equations, would result in negative values for these parameters, which is impossible. It is this point which is associated with the λ transition. It is interesting to note that the probabilities for both the short-sided polygons (except the two-sided ones) and all the long-sided polygons become zero at the same temperature. The only polygons which can exist (using these equations) above this temperature are the double-sided ones, in agreement with the results of (I).

Analytical conditions for the λ point may be obtained by setting z_5 and z_{10} equal to zero in Eqs. (6.1) and (6.5); two simultaneous conditions on τ_λ result:

$$\tau_\lambda=\ln[(\alpha_\lambda^2-5)/\alpha_\lambda], \tag{7.1}$$

$$B_\lambda=(\alpha_\lambda-5)(\alpha_\lambda^2+1)/[(\alpha_\lambda^2-5)(\alpha_\lambda+1)], \tag{7.2}$$

where B_λ is B of (5.15) with τ_λ replacing τ. When these equations are solved numerically, one obtains

$$\tau_\lambda=1.886, \tag{7.3}$$

$$\alpha_\lambda=7.278. \tag{7.4}$$

This value of τ_λ may be compared with the result of (I) which is, in the present notation,

$$\tau_\lambda=1.386. \tag{7.5}$$

If the observed λ point temperature, 2.19°K, is used with the result (7.3) and Eq. (5.5), and if 3.58 A (the average distance between atoms in liquid helium at the λ point) is used as the value of c, the effective mass m' is found to be about 1.57 times that of the He atom. This result agrees with that expected by Feynman.[3]

8. ASYMPTOTIC RESULTS NEAR 0°K

Using Eq. (5.15), the asymptotic expressions for B and $\partial \ln B/\partial\tau$ near 0°K become

$$B=(\pi/\tau)^{\frac{3}{2}}-1-6e^{-\tau}+O(\exp(-\pi^2/\tau)), \tag{8.1}$$

$$\frac{\partial}{\partial\tau}\ln B=-\frac{3}{2}\frac{1}{B}[\tfrac{3}{2}+9e^{-\tau}-6\tau e^{-\tau}] +O(\exp(-\pi^2/\tau)). \tag{8.2}$$

Also, from (6.2), since B becomes infinite as $\tau^{-\frac{3}{2}}$ as τ approaches zero, the asymptotic form for α in this region becomes

$$\alpha=Be^{\tau}+4+O(1/B). \tag{8.3}$$

Substituting these results into the expressions for x_4, x_5, y_4, y_8, y_{17}, and y_{18} given in Eq. (6.5), one obtains for the energy E of (6.8) under these conditions

$$E/NkT=3(1+6e^{-2\tau}-4\tau e^{-2\tau})/2B^2+O(1/B^3). \tag{8.4}$$

Using (8.1), one obtains

$$E/NkT=21\tau^3/(2\pi^3)+O(\tau^4). \tag{8.5}$$

Since τ is directly proportional to T, E varies as T^4 near 0°K. From (8.5), one obtains the specific heat near 0°K as

$$C_v/Nk=(42/\pi^3)\tau^3+O(\tau^4). \tag{8.6}$$

This expression qualitatively agrees with the experimental results for low temperatures[8] in the sense that C_v becomes zero at 0°K with a horizontal tangent. Although one is tempted to emphasize the T^3 dependence in (8.6), this particular functional form is probably fortuitous, because (i) the present theory does not take into account the phonons, which cause the experimental T^3 specific heat, (ii) the temperature variation of K_β was neglected, and (iii) the coefficient of T^3 in (8.6) is two orders of magnitude larger than the experimental value.[8] Nevertheless, it should be emphasized here that as the combinatorial aspect of the treatment is concerned, the approximation becomes more and more accurate with the decreasing temperature and approaches the exact analysis at 0°K, since the infinitely long sides predominate at the lowest temperatures.

9. THE SPECIFIC HEAT BELOW THE λ POINT

In order to obtain the energy and specific heat between 0°K and the λ point, first B of Eq. (5.15) is

[8] A. H. Markham, D. C. Pearce, R. G. Netzel, and J. D. Dillinger, *Proceedings of the Fifth International Conference on Low-Temperature Physics*, edited by J. D. Dillinger (University of Wisconsin Press, Madison, 1958), p. 45.

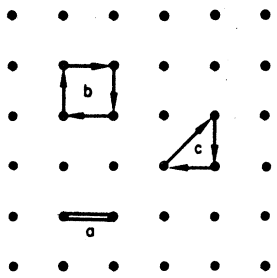

FIG. 7. Small finite polygons assumed to exist above T_λ. a: double-bond, b: square, and c: triangle.

calculated for a given value of τ, and then (6.2) is solved for α. The probability parameters are calculated from (6.5). The factor $\partial \ln B/\partial\tau$ is also evaluated by means of the expansion (5.15) in the form $(1/B)\partial B/\partial\tau$. When these results are substituted into (6.8) and the first term involving K_β is neglected as mentioned before, the energy E is obtained as a function of the temperature T. Numerical differentiation of this energy yielded the curve for the specific heat at constant volume C_v, which is shown by the solid line between 0 and τ_λ in Fig. 6. This numerical work was done on the IBM-650 digital computer at the Wayne State University Computation Center.

10. ABOVE THE λ POINT

As was pointed out in Sec. 7, above the λ point the preceding treatment leads to exactly the same results as those of the previous calculation (I), since in both cases the only polygons assumed to exist above T_λ are the double-sided ones. The larger value of τ_λ found in this work [compared with that of (I)] removes most of the rapidly ascending portion of the specific heat curve of (I) just above T_λ, as is seen in Fig. 6. Nevertheless a slight rise in C_v above the new T_λ still remains. This result does not agree with the experimental observation (and the conclusion derived by Feynman[3]) that the specific heat decreases monotonically above the λ point.

The unsatisfactory behavior of C_v just above T_λ obtained here is interpreted as due to the fact that all of the finite-sized polygons which are suspected to exist above T_λ are excluded in the treatment except the smallest ones, i.e., the double-sided polyogons (which we shall call "double-bonds"). Following this interpretation, a study of the possible existence of

CONFIGURATION OF A POINT	PROBABILITY	WEIGHT γ_i
•	v_1	1
⊃	v_2	6
⊥	v_3	24
↘	v_4	48

FIG. 8. Point probability parameters including point, double-bonds and triangles only. A dotted line is the hypotenuse (of length $\sqrt{2}c$) of an isosceles right triangle.

CONFIGURATION OF A BOND	PROBABILITY	WEIGHT δ_i
• •	w_1	1
• ═	w_2	10
═ ‖	w_3	25
⬭	w_4	1
• ⌐	w_5	32
⊃ ⌐	w_6	160
⊣ ⌐	w_7	256
• ⟋	w_8	80
⊃ ⟋	w_9	80
‖ ⟋	w_{10}	256

(a

CONFIGURATION OF A BOND	PROBABILITY	WEIGHT δ_i
‖ ↘	w_{11}	48
⊣ ⟋	w_{12}	1024
→ ↘	w_{13}	96
↓ ↘	w_{14}	64
↘ ⌐	w_{15}	1024
⟋ ⌐	w_{16}	128
⟋ ↳	w_{17}	288
⟋ ⟋	w_{18}	48
⌐ ↘	w_{19}	16

(b)

FIG. 9. Pair probability parameters including points, double-bonds and triangles only.

finite polygons other than the double-bonds was made for temperatures above T_λ. In order to secure mathematical simplicity, only square and triangular polygons like those shown in Fig. 7 were introduced. Since the virtual energies E^* of these figures are lower than all other finite polygons, except a double-sided polygon between *second* nearest-neighbors, their effects would be next in importance to those of the double-bonds at temperatures above T_λ. The mathematical treatment was formulated using a modification of the pair approximation of the previous sections.

A calculation showed that the square polygons could not exist with the double-bonds above the transition

temperature. A possible explanation of this result is that the virtual entropy S^* associated with the combinatorial factor for this symmetrical figure is too low compared to the virtual energy, and therefore minimization of the free energy led to its disappearance.

A study of the system of double-bonds and triangles was then made with the result that such a system was found stable at temperatures above T_λ. The lack of symmetry in the triangle perhaps made the virtual entropy contribution of the figure dominate over its virtual energy (which equals the virtual energy of a square). The effects of the existence of such triangles on the specific heat curve in the high temperature region will be discussed in this section.

A new set of configuration variables is defined in Figs. 8 and 9. It should be noted that in this new system the only existing polygons are double-bonds and triangles, all larger polygons being excluded. Although these figures have some configurations in common with Figs. 2 to 4, the weight factors for the same configurations are not necessarily equal. For instance, the weight 24 for v_3 in Fig. 8 counts only the perpendicular arrows which form two sides of a triangle, whereas the weight 30 for x_3 in Fig. 4 includes the two arrows pointing in the same direction. Because of the existence of the dotted sides, which represent the hypotenuses of the right triangles, subtle differences appear among w_9, w_{10}, and w_{11}, among w_{12}, w_{13}, and w_{14}, and among w_{15}, w_{16}, w_{17}, and w_{18}. For instance, in w_{10}, the dotted side lies away from the bond, whereas in w_{11} it lies towards the bond. In counting the weight for w_{11} the configuration in which the double-bond and the dotted side have a common lattice point must be omitted.

Among the new variables the following relations exist.

$$\begin{aligned}
1&=v_1+6v_2+24v_3+48v_4,\\
v_1&=w_1+5w_2+16w_5+40w_8,\\
v_2&=w_2+5w_3+16w_6+40w_9\\
&=w_2+5w_3+16w_6+32w_{10}+6w_{11}\\
&=w_4,\\
v_3&=w_5+5w_6+16w_7+32w_{12}+6w_{13}\\
&=w_5+5w_6+16w_7+32w_{12}+4w_{14}\\
&=w_{19},\\
v_4&=w_8+w_9+4w_{10}+16w_{12}+32w_{15}+8w_{16}\\
&=w_8+w_9+4w_{10}+16w_{12}+32w_{15}+6w_{17}\\
&=w_8+w_9+3w_{11}+6w_{13}+4w_{14}+8w_{16}+18w_{17}+6w_{18}\\
&=w_{19}.
\end{aligned} \tag{10.1}$$

The total equivalent number of short sides of length c (the lattice constant) is now given by $3N(2w_4+32w_{19})$ since each w_{19} bound is related to one-half of the four "equivalent sides" of a triangle.[9] Therefore, corresponding to (5.3), the free energy in this case is written as

$$\begin{aligned}
F/kT=&-\ln[K_\beta N!^{-1}(m'kT/2\pi\hbar^2)^{3N/2}]\\
&+3N\tau(2w_4+32w_{19})-5N\sum_{i=1}^{4}\gamma_i v_i\ln v_i\\
&+3N\sum_{i=1}^{19}\delta_i w_i\ln w_i.
\end{aligned} \tag{10.2}$$

Because of the relations in (10.1), only 11 variables of the four v's and 19 w's are independent. A set of eleven of these variables is chosen appropriately, and the free energy (10.2) is minimized. A set of nonlinear simultaneous equations is obtained, which may be written in the following form.

$$\begin{aligned}
&[56+(9/2A)(f+g-2b+10d+4p/9-7d^2/4A\\
&\quad-9bd/A)]u_8^{\frac{3}{4}}+[5+(9/2A)(d+2be^{-2\tau})]u_8\\
&\quad+u_8^{\frac{1}{4}}-2e^{-2\tau}=0,
\end{aligned} \tag{10.3}$$

$$\begin{aligned}
&\theta^{10}+(u_2K^{-1/4}/8+u_5/2)\theta^9/u_8-(3/4)^{7/4}\theta^5\\
&\quad-3[u_2K^{-1/4}/32+(2/3)^{\frac{1}{4}}u_5]\theta^4/u_8-3/16=0,
\end{aligned} \tag{10.4}$$

where $u_i=w_i/w_1$ for $i=2,\cdots,19$, and

$$\begin{aligned}
\theta&=u_{15}^{\frac{1}{4}}/u_8,\\
A&=1+5u_2+16u_5+40u_8,\\
K&=(4\theta/5+3\theta^{-4}/20)^{4/5},\\
b&=40(1-K),\\
p&=40-32\theta-(2/3)^{\frac{1}{4}}6/\theta^4,\\
d&=5-K-\theta K^{-1/4},\\
f&=16(1-\theta),\\
g&=40-32\theta^2-(3/4)^{3/4}8/\theta^3,\\
u_2&=(1-9bu_8/A)e^{-2\tau}/A,\\
u_5&=u_8[1-u_2dA^{-1}-u_8(f+g-c)A^{-1}].
\end{aligned} \tag{10.5}$$

In deriving (10.3), the quantities of order $(u_8/A)^2$ are neglected with respect to unity. This is justified since it can be shown that u_8 is smaller than 10^{-3} above T_λ, and A is always larger than unity.

The numerical computation is done as follows. When a set of test values of K, u_2, u_5 and u_8 is chosen,[10] (10.4) is solved for θ. Next (10.3) is solved for u_8. New values of the parameters in (10.5) are calculated, and this procedure is repeated iteratively until u_8 is determined to four significant figures.

After these equations are solved the specific heat is derived as follows. By analogy to (6.8), the energy of the system is expressible as

$$E=NkT[\tfrac{3}{2}-3\tau(2w_4+32w_{19})],$$

[9] The virtual energy associated with one triangle is $(m'k^2T^2/2\hbar^2)\times(2c^2+(\sqrt{2}c)^2)=4\epsilon_c^*$.

[10] The first trial set is chosen by solving (10.3) with all the terms of order $1/A$ dropped.

where

$$w_4=w_1u_2(1-bu_8A^{-1}),$$
$$w_{19}=w_1u_5(1-u_8A^{-1}), \tag{10.7}$$
$$w_1^{-1}=1+6u_2+24u_5+48u_8+6(8d-b)u_2u_8A^{-1}.$$

The specific heat C_v is derived from E of (10.7) by numerical differentiation. The result is shown by the dot-dash curve in Fig. 6. Although C_v is still slightly ascending for $\tau<2$, the general shape of the new C_v curve is better than the solid curve of the previous calculation. This indicates the correctness of the interpretation that the specific heat curve above T_λ will approach the experimental behavior when more finite polygons are added in this treatment.

It must be noted here that the calculation in this section is only for the region above T_λ, and the value of the λ point has not been calculated in the approximation corresponding to this section. In order to do this the triangles of this section must be combined with the long sides of the previous sections, which would require considerable additional calculation.

Nevertheless, without expending more mathematical effort, based on what was found in this section and also in previous sections, the shape of the specific heat curve for a more accurate treatment of the model can be inferred as follows. The solid curve in Fig. 6 for the very low temperatures, probably below $\tau=1$, will remain practically the same in better approximations, because near absolute zero the very long sides are predominant and the approximation in this paper is good. As the approximation is improved, the curve right above T_λ will increase as was shown in this section. This will induce the lowering of the λ point because the total area below the C_v curve must remain the same in order to keep the same values of energy at 0°K and at temperatures well above T_λ. It is a general tendency of cooperative phenomena that the peak of the specific heat becomes higher as the approximation is improved, and so this will probably be the case in the present model.

11. SUMMARY AND CONCLUSION

The partition function for liquid He⁴ proposed by Feynman, Eq. (7) of reference 3, based on his path integral method, was evaluated for a simple cubic structure previously by Kikuchi,[4] considering only nearest-neighbor permutations of the atoms. In this paper the same partition function is evaluated considering long-range permutations as well. The result is plotted in Fig. 6. It indicates a second order phase transition, and the value for the effective mass of a helium atom becomes about 1.6 times the normal mass, if the theoretical T_λ is equated with the experimental point. The marked improvements of the present work compared with the previous work[4] are (1) the specific heat varies as T^3 near absolute zero, (2) the peak of C_v at T_λ is more pronounced than in (I), and (3) when triangles are added as possible finite polygons above T_λ, the specific heat just above T_λ increases over the previous result, indicating an improvement.

It is now concluded that Feynman's partition function calculated on a lattice gives a satisfactory qualitative picture of the λ transition of liquid He⁴, and also that the technique for handling the long-range permutations of atoms developed in this paper is correct.

ACKNOWLEDGMENTS

The authors wish to acknowledge the assistance of William I. Ginsberg in some of the calculations, and of Marcos F. Maestre who programmed the numerical calculations discussed in Sec. 9. The assistance of the Computation Center of Wayne State University in granting clerical aid and digital computer time is also gratefully acknowledged.